Journal of Thermal Analysis and Calorimetry, Vol. 84 (2006) 2, 307–316

THERMAL CONDUCTANCE MEASUREMENTS OF SUPERCONDUCTING Bi-2212 RODS AND A Bi-2212-BASED CURRENT LEAD MODULE
Analysis and results

*Eva Natividad, M. Castro**, *R. Burriel and L. A. Angurel*

Instituto de Ciencia de Materiales de Aragón (CSIC – Universidad de Zaragoza) Edificio Torres Quevedo, Sede CPS, María de Luna 3, 50018 Zaragoza, Spain

We measured from 5 to 300 K the thermal conductance of different superconducting Bi-2212 thin rods and one superconducting module integrating a hybrid current lead based on such rods. The conductance values of the rods are lower than the measurable limits of the set-up and a detailed evaluation of the heat losses is required. The analysis of the heat exchanges permits to introduce a correction function to the measured values and allows to study low thermal conductivity materials. The dependence of the thermal conductivity of Bi-2212 rods on the sample microstructure is analyzed after this correction. We calculate analytically the time required to reach the steady-state for long bars for which extended relaxation times are expected. From the measured conductance data we estimate the heat load introduced by the current lead into a cryogenic bath in static conditions.

Keywords: *current lead, high-T_c superconductors, longitudinal steady-state method, thermal conductivity, thermal losses, thermal relaxation time*

Introduction

The transfer of high currents from room-temperature power generation sources to low-temperature superconducting devices requires the use of current leads. These current leads introduce a heat load into the cooling source or bath that represents a non-negligible energy waste. The main sources of this load are the electrical resistance of the leads, which generates Joule dissipation during operation, and their thermal conductance, which causes heat transfer even in static conditions. In the case of conventional all-metal current leads, the predominant electronic contribution to the transport properties gives a strong correlation of the electric and thermal conductivities, and the driving of high currents originates important heat loads. However, hybrid metal/HTS (high temperature superconductor) leads [1], consisting of a metallic high-temperature part and a HTS low-temperature part, transfer current with strongly reduced losses due to the poor thermal conductivity and lack of Joule dissipation of the superconducting part at temperatures below the critical temperature, T_c. During the last years, several companies have commercialized high-performance hybrid current leads. Most of them use Bi-based HTS: $(Bi,Pb)_2Sr_2Ca_2Cu_3O_{10+\delta}$ (Bi-2223) bulk materials (for instance, CAN Superconductors), Ag–Au/Bi-2223 composite tapes (CryoSaver^{TM} of HTS-110 with technology of American Superconductors, American Magnetics), $Bi_2Sr_2CaCu_2O_{8+\delta}$ (Bi-2212) melt cast processed monoliths (Nexans Superconductor and ACCEL Instruments) or Bi-2212 dip coated plates (Oxford Instruments). Several prototypes based on $YBa_2Cu_3O_{7-\delta}$ materials (Eurus or Haldor Topsoe, for instance) were investigated but they showed poorer performance in this application than Bi-based materials. Other hybrid systems currently under study are Peltier current leads [2], which use thermoelectric semiconductors instead of metals, allowing an additional reduction of the heat leak.

During the design and construction of the large hadron collider (LHC), CERN made an international R&D call to be supplied of high-performance hybrid current leads [3] for feeding its 8000 superconducting magnets operating at helium temperature. A collaboration was established to design and fabricate a 600 A prototype [4], according to CERN specifications between our group, the superconductivity group at the Spanish CEDEX-CIEMAT, and the company ANTEC. The superconducting part of this lead was formed by four superconducting modules based on Bi-2212 thin rods textured by the laser floating zone (LFZ) technique [5]. The value of the heat load at the cold end of the low-T part is an important technical specification in these leads. Therefore, it was necessary to determine, on one hand, the thermal conductivity (κ) of the rods and its dependence with processing parameters and microstructure, and, on the other hand, the value of the thermal conductance (K) of each superconducting module.

* Author for correspondence: mcastro@unizar.es

1388–6150/$20.00

Akadémiai Kiadó, Budapest, Hungary
Springer, Dordrecht, The Netherlands

A commercial installation from Termis Ltd. was used for the thermal conductivity measurements [6]. This set-up, based on the longitudinal steady-state method, provides direct thermal conductance values in the temperature range 1.5–375 K, allowing a straightforward determination of the total heat load between two different temperatures. This is clearly an advantage of steady-state methods compared to transient or modulated techniques. However, two difficulties were encountered when measuring the superconducting rods and the modules: *i*) The measured thermal conductivity values of the rods were next to or lower than the set-up lower limit; *ii*) The superconducting module was much longer than the sample space available in the commercial thermal conductance cell.

In the present work, we report the corrections performed on the thermal conductance data of the individual superconducting rods, in order to subtract the detected error contributions to the measurements, unimportant in the case of higher K values. We also describe a new cell designed and fabricated to hold the superconducting module and similar units, as well as the calculation of the relaxation time of the new system to steady-state conditions. Measurement results of the individual rods and the hybrid current-lead module are presented.

Experimental

Brief description of the set-up

The thermal conductance measurements were performed in a commercial installation (Termis Ltd.), described in detail in [6]. Basically, it is a modular apparatus consisting of a head, which contains the vacuum and electrical connections, the measuring cell and a long stem that connects both parts and allows the cell to be immersed in liquid nitrogen or helium. The sealing of the working space is made through an outer jacket joined to the stem with a white silicone paste. This is a versatile installation that can perform different kind of measurements (heat capacity, thermal conductance or thermometer/thermocouple calibration) just by changing the measuring cell.

In particular, the commercial thermal conductivity cell can measure thermal conductance with a sensitivity varying from 1 μW K^{-1} at 1.5 K to 10 μW K^{-1} at 300 K and with a temperature resolution of 1 mK. The nominal minimum/maximum K values that can be directly determined are, respectively, 30 μW K^{-1}/1 mW K^{-1} at 1.5 K, and 1 mW K^{-1}/100 mW K^{-1} at 300 K. The sample size (cylindrical or prismatic specimen) must be between 1 and 15 mm in diameter and 2 and 22 mm in height.

The installation includes a measuring-control and data-acquisition system together with an interactive program, which allows fully programming the experiments.

Thermal conductance measurement process

As mentioned before, the thermal conductance measurements are performed using a longitudinal steady-state method. Briefly, temperature differences are induced between both ends of the sample by the action of two heaters on the source (high T) and sink (low T). Measurements of the thermal flow and the temperatures of source and sink are carried out. The heat losses from the source are minimized by a lateral radiation shield. Under stationary conditions, the thermal conductance is calculated from the ratio of the heat power supplied by the source, P, and the temperature difference between source and sink, ΔT. For samples with well-defined geometries, the thermal conductivity can be calculated from the expression $\kappa=KL/A$, where L and A are the length and the cross-section of the sample, respectively.

In practice, the thermal conductance value at a fixed temperature is determined in two steps. During the first step, the source, radiation shield and sink must reach certain temperatures, namely, $T_{source,1}=T_{shield,1}=T_{set}$ and $T_{sink,1}=T_{set}-\delta_1$, where T_{set} is the temperature set point, and the parameter δ_1 accounts for a fixed temperature difference between source and sink, $\Delta T_1=T_{source,1}-T_{sink,1}=\delta_1$, necessary to maintain a stationary state. Once the system fulfils the stationary condition with stable temperatures, the heating power of the source, $P_{source,1}$, is recorded. This heating power includes the heat flow through the sample as well as every unaccounted heat exchanges between the source block, the shield and the sample. The second step is similar to the first one except for the temperature differences. T_{sink} remains unchanged, but the source and shield temperatures are increased to $T_{source,2}=T_{shield,2}=T_{set}+\delta_2$, resulting in a temperature difference between source and sink $\Delta T_2=T_{source,2}-T_{sink,2}=\delta_2+\delta_1$. Under stationary conditions, a new power value, $P_{source,2}$, is measured. From these two steps, K can be determined by a differential method that allows discarding every constant or small spurious contribution. The additional heat power supplied by the source is defined as $P=P_{source,2}-P_{source,1}$, the temperature difference as $\Delta T=\Delta T_2-\Delta T_1=\delta_2$ and, in consequence, the thermal conductance is calculated as $K=P/\Delta T$. Finally, the mean temperature of the whole process, defined as $T_{mean}=(T_{source,1}+T_{sink,1}+T_{source,2}+T_{sink,2})/4=T_{set}+(\delta_2-2\delta_1)/4$, is associated to the obtained K value.

Thermal conductivity of the superconducting rods

Measuring cell and samples

The thermal conductance of the superconducting rods was measured in the commercial cell, shown in Fig. 1. The source and sink are two well-polished oxygen-free copper blocks with an area $A_{source}=A_{sink}=1.767\cdot10^{-4}$ m^2, and the radiation shield (not shown) is a copper cylinder thermally controlled at the source temperature and extending up to the sink. Samples of 1 cm in length and about 1.6 mm in diameter were measured in the temperature range 5–300 K. Usually, the thermal contact is achieved between the sample base and the copper blocks by pressing and the addition of thermal-contact grease. However, to avoid contact problems arising from a bad alignment due to the small cross-section of the rods (about 2 mm^2), the contacts sample-sink and sample-source were improved using two copper pieces (Fig. 1) with larger cross-section (ϕ=5 mm) and indium-plated on the contact surfaces. These pieces were soldered to the rod ends using Wood's metal and finally pressed to the source and sink surfaces, previously wetted with thermal grease.

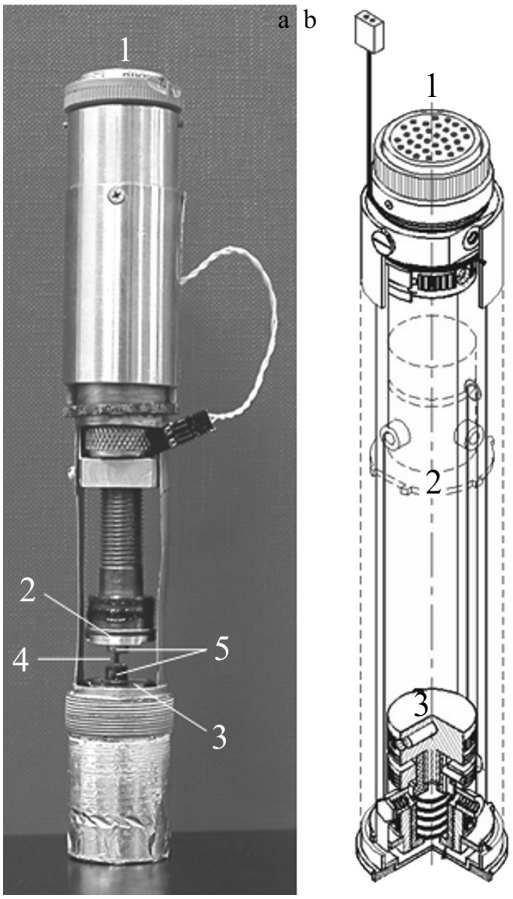

Fig. 1 a – Photograph of the commercial thermal conductivity cell showing the 1 – electrical connector and a 4 – Bi-2212 rod with 5 – contact copper pieces soldered to the ends of the rod and located between 2 – sink and 3 – source. b – Sketch of the bigger-sized thermal conductance cell showing the 1 – electrical connector, 2 – the sink and 3 – source

Table 1 Measured and estimated conductance contributions (in μW K^{-1}) at several temperatures and ΔT values used for specimens of 1.6 mm in diameter and 1 cm long: measured K data of a Bi-2212 thin rod, estimated upper limit of the rod-shield ($P_{rad,L}/\Delta T$) and source-sink ($P_{rad,S}/\Delta T$) radiation loss contribution to K, and thermal conductance measurements (K_{wood}) performed with a wood spacer (see text)

T_{source}/K	ΔT/K	K	$P_{rad,L}/\Delta T$	$P_{rad,S}/\Delta T$	K_{wood}
20	0.4	325.6	–0.05	0.28	15
50	0.8	600.0	–0.70	4.3	21
80	2.0	750.6	–2.8	17.6	32
150	3.0	832.2	–18.9	116.6	89
200	3.0	997.5	–44.9	278.5	170
300	3.0	1513	–152.4	947.2	489

Corrections to the K measurements

Preliminary measurements on Bi-2212 thin rods showed that K ranged between 0.2 mW K^{-1} at 10 K and 1.5 mW K^{-1} at 300 K (Table 1), close to the measurable lower limit of the set-up. Due to that, we evaluated the heat losses that usually represent negligible contributions to the total conductance, but might be important in the case of low-K measurements. It is necessary to detect and infer the origin of these eventual losses and elaborate a correction function based on the measuring process.

Heat-loss sources

Gas conduction and convection losses are assumed to be negligible, since the sample chamber is under vacuum during the measurements. Then, possible losses can be initially ascribed to two main sources: *i*) radiation heat interchange between the sample lateral surface and the shield; *ii*) radiation between source and sink, since the small sample section leaves uncovered a broad area of these surfaces. A calculation of each case is performed in order to estimate their contributions to the measured K.

Considering the radiation between the sample lateral surface and the shield, the differential radiation power equation can be written as:

$$dP_{rad,L} = \sigma\varepsilon_{12}\,[T_s(x)^4 - T_{shield}^4]\,dA_L \qquad (1)$$

where σ is the Stefan–Boltzman constant, ε_{12} is the sample-shield combined emissivity, $T_s(x)$ stands for the temperature distribution along the sample and $dA_L=2\pi R dx$ is its differential lateral area. Under sta-

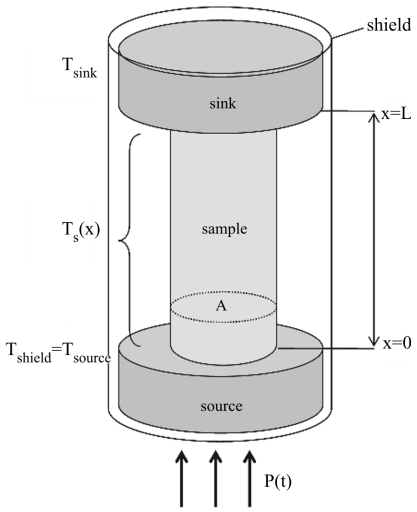

Fig. 2 Thermal model used for the analytical calculations

tionary conditions, the temperature distribution along the sample is given by:

$$T_s(x)=T_{source}-(\Delta T_i/L)x \quad (2)$$

where x is the length variable along the rod axis, x=0 is the source position and x=L is the sink position, as shown in Fig. 2. In this expression, $\Delta T_i = T_{source,i}-T_{sink,i}$ (i=1, 2, depending on the measuring step), and $T_{shield}=T_{source}$, since the shield is maintained at the source temperature.

Then, the total radiation power, calculated by integrating Eq. (1), results

$$P_{rad,L}=2\pi R\sigma\varepsilon_{12}\int_0^L (T_s(x)^4 - T_{shield}^4)dx \quad (3)$$

A positive value of this integral indicates that a radiation flux exists from the sample to the shield. In such a case, the source block would need more heating power to keep a constant temperature, and the measured sample conductance would be higher than the real one. Contrarily, a negative integral value would derive a lower apparent conductance of the sample.

The contribution of the radiation between source and sink, $P_{rad,S}$, can be estimated from the following equation

$$P_{rad,S}=\sigma A_S\varepsilon'_{12}(T_{source}^4 - T_{sink}^4) \quad (4)$$

where A_S stands for the area of the sink and source, except for the fraction occupied by the sample, that is, $A_S=A_{source}-A$, and ε'_{12} is the source–sink combined emissivity. In this case, a positive value indicates a radiation flux from the source to the sink and, as in the previous case, the measured sample conductance would be higher than the real one.

Eventually, the total radiation power can be expressed as

$$P_{rad,T}=P_{rad,L}+P_{rad,S} \quad (5)$$

The radiation loss is negligible when $P_{rad,T}<<P_i=K\Delta T_i$, being P_i the measured heat power in each step explained in 'Thermal conductance measurement process'. Table 1 collects the upper limits of $P_{rad,L}$ and $P_{rad,S}$ at several temperatures, considering ε_{12}=1, R=8·10^{-4} m (thickest rod), L=10^{-2} m, and A_s = 1.57·10^{-4} m^2. $P_{rad,L}$ is negative and $P_{rad,S}$ positive, indicating heat radiation fluxes from the shield to the sample and from the source to the sink, respectively. Moreover, the maximum contribution of the source–sink radiation is almost one order of magnitude higher than the contribution of the shield–rod radiation, due to the sample geometry. The lateral radiation losses contribute less than 10% to the measured K values in the whole temperature range and cannot be considered an important error. However, the source–sink radiation contribution is an important source of error in the measurements, increasing its influence at higher temperatures.

Correction function

In order to quantify radiation losses, thermal conductance measurements (K_{wood}) were performed in the whole temperature range using a sample-sized wood spacer between source and sink. The use of a fake material assures maintaining the same tension and geometry to provide similar heat conducting conditions of the cell body as existing with a real sample. Due to the low thermal conductivity of wood (0.04–0.35 W m^{-1} K^{-1} at

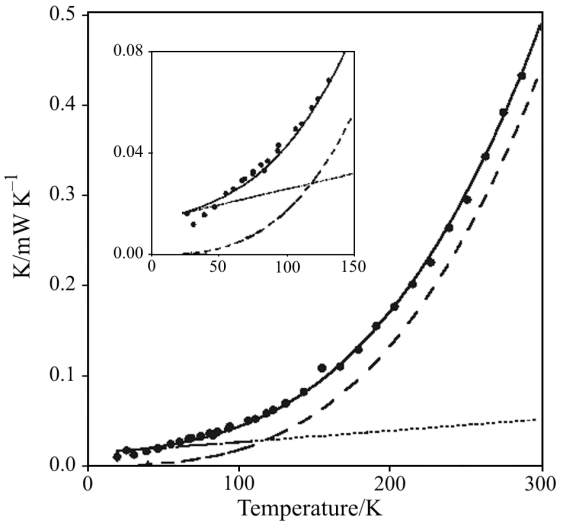

Fig. 3 Measured thermal conductance (points) with the wood spacer K_{wood}, together with the fit to Eq. (8) (continuous line). The dashed line stands for the contribution of radiation losses between source and sink, K_{rad}, calculated from Eq. (7). The dotted line describes the linear contribution assigned to the wood conductance. The inset shows a detail of the low temperature region

300 K [7]) the measured heat flow is mainly due to source-sink radiation losses. The results are depicted in Fig. 3. In addition, some of the data are collected in Table 1 for a better comparison with the other values. Clearly, the shape and magnitude of the curve indicate that the source–sink radiation loss is the main contribution, corresponding to an important fraction of the measured rod conductance at high temperature. However, the contribution of the thermal conductance through the wood spacer may not be negligible in these results. In effect, reported κ values [8] for birch wood with zero moisture content and measured in the radial direction vary between 0.14 and 0.18 W m^{-1} K^{-1} at 233 and 373 K, respectively, showing a linear increasing trend with temperature. For a wood sample of $R=8\cdot10^{-4}$ m and $L=10^{-2}$ m, the thermal conductance at 233 K would be 27 μW K^{-1}, that is, 11% of the total measured values (Fig. 3) at this temperature. In addition, this percentage is expected to grow with decreasing temperature, since the radiation contribution falls rapidly with T.

In order to obtain a correction function for the radiation losses, we express the Stefan law in terms of the measuring parameters. Neglecting $P_{rad,L}$, considering Eq. (4), and taking into account that the final measured losses, P_{rad}, correspond to the difference between the losses in the first and second steps, we obtain

$$P_{rad} \cong P_{rad,S,2} - P_{rad,S,1} = c_1(T^4_{source,2} - T^4_{sink,2}) - \\ -c_1(T^4_{source,1} - T^4_{sink,1}) \quad (6)$$

where $c_1=\sigma A_S \varepsilon'_{12}$.

From thermal conductance measuring process, $T_{sink,1}=T_{sink,2}$, $T_{source,1}=T_{set}$ and $T_{source,2}=T_{set}+\delta_2$. In addition, since we chose δ_1 to have the value $\delta_2/2$ in our experiments, $T_{mean}=T_{set}\equiv T$. Therefore, the conductance contribution due to radiation losses, K_{rad}, can be expressed as

$$K_{rad}=P_{rad}/\Delta T \cong c_1(4T^3+6T^2\Delta T+4T\Delta T^2+\Delta T^3) \quad (7)$$

and the experimental conductance measured with wood must be fitted with the following function

$$K_{wood}=K_{rad}(T,\Delta T)+c_2T+c_3 \quad (8)$$

where the second and third terms account for the linear contribution of the wood spacer. This linear trend is only an extrapolation of the high-T results and is expected not to be valid for very low T, where the term c_3 would have no physical sense.

By fitting the experimental data to Eq. (8) with ΔT=6 K (used value), we obtain $c_1=3.94\cdot10^{-12}$ W K^{-4}, $c_2=1.25\cdot10^{-7}$ W K^{-2}, and $c_3=1.33\cdot10^{-5}$ W K^{-1}. This drives to the value $\varepsilon'_{12}=0.44$ for the sink-source emissivity, and to $\kappa=0.25$ W m^{-1} K^{-1} for the conductivity of wood at 300 K, which are in the expected range. The fit reproduces the experimental data down to 50 K. Below this temperature, the experimental K increases its slope and tends to zero and it can no longer be described by the second and third terms of Eq. (8). However, the difference between the experimental K for wood and the fit at these temperatures represents less than 5% of the conductance data measured for the Bi-2212 rods. Therefore, we can take Eq. (8) as valid for the whole temperature range. Then, with these three parameters, the correction function is already defined, and the real conductance values of the rods, K_{real}, are given by

$$K_{real}=K-K_{rad}(T,\Delta T) \quad (9)$$

where K is the measured value and K_{rad} is the correction function.

Eventually, the thermal conductivity of the Bi-2212 rods must be calculated from the real conductance values according to the expression

$$\kappa=(L/A)K_{real}=(L/A)[K-\sigma(A_{source}-A)\varepsilon'_{12} \\ \cdot(4T^3+6T^2\Delta T+4T\Delta T^2+\Delta T^3)] \quad (10)$$

where L and A are the length and cross-section of the rod, respectively, K the measured conductance values, A_{source} the area of the source (or sink), ε'_{12} the source-sink combined emissivity, T the temperature associated to each K value, and ΔT the final temperature difference of each measured point ('Thermal conductance measurement process'). Note that, for our set-up, $A_{source}=1.767\cdot10^{-4}$ m^2 and $\varepsilon'_{12}=0.44$. Therefore, this method can be applied to the determination of the thermal conductivity of any material just taking into account its geometry and the new experimental conditions.

Measurement results for the rods

The uncorrected and corrected thermal conductance values for one Bi-2212 thin rod of 1.6 mm in diameter

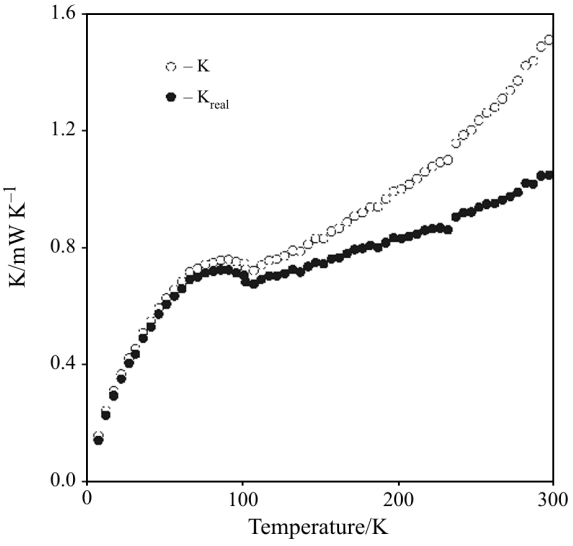

Fig. 4 Measured (K) and corrected (K_{real}) thermal conductance values of one rod of 1.6 mm in diameter and 1 cm long

and 1 cm in length are shown in Fig. 4. The uncorrected K values show a non-linear increasing trend above 100 K caused by radiation losses, and becomes almost linear after correction. We apply this correction to the conductance measurements on several Bi-2212 rods obtained with different processing conditions. The results allow us to study the dependence of κ with the sample microstructure [9], characterized by SEM and EDX analysis.

The LFZ texturing process generates thin rods whose Bi-2212 crystallites are oriented with their *a–b* planes almost parallel to the growing direction, that is, the rod axis. This orientation allows obtaining the highest current-driving potential. Since the thermal conductivity was measured along this axis, we can assume that the $\kappa_{ab}(T)$ component represents the major contribution to the measured $\kappa(T)$. However, other factors, like granularity, variations in the Bi-2212 phase composition or presence of Bi-free non-superconducting secondary phases [9] can also influence these κ values.

The variation of the thermal conductivity with temperature, $\kappa(T)$, of three different rods in the range 5–200 K is depicted in Fig. 5. In fact the measurement range was 5–300 K but, given that the radiation losses represent more than 20% of the measured K values at temperatures above 200 K, only κ data values under this temperature are here considered. The qualitative behaviour is similar for every sample: In the normal state ($T>T_c$, where T_c varies between 83.5 and 92.1 K), the conductivities follow parallel trends, with a weak temperature dependence. Below T_c, they show a slight upturn, reach a maximum and decrease sharply with temperature. This trend is typical of superconductors of this kind [10–14]. However, the κ values differ in more than 50% (2.90 W m^{-1} K^{-1} for sample a *vs.* 1.62 W/m K for sample c at 150 K). Variations of the same order are found in the literature for similar Bi-2212 bulk samples: about 3.7 W m^{-1} K^{-1} at 150 K for single crystals [10, 11], 3.2 W m^{-1} K^{-1} for floating zone (FZ) textured bars [12], 2.0 W m^{-1} K^{-1} for melt-cast rods [13], and 4.5 W m^{-1} K^{-1} at 100 K for melt-cast tubes [14]. In our case, the differences observed in Fig. 5 are attributed to the presence of Bi-free non-superconducting precipitates within the samples [9]. The microstructural analysis allows quantifying the volume content of these precipitates, being always <10% of the whole rod volume. For these concentrations, $\kappa(T)$ of the whole rod was found to be governed by the rule of mixtures, usually obeyed for small concentrations of particles dispersed inside a matrix [9, 12]. From the precipitates concentration of samples a and b, 6.8 and 4.9%, resprctively, the estimated thermal conductivity of these precipitates is 26.3 W m^{-1} K^{-1} at 150 K. The conductivity $\kappa(T)$ for the Bi-2212 phase of a LFZ-textured polycrystalline sample corresponds to the values of sample c, which is free of non-superconducting precipitates.

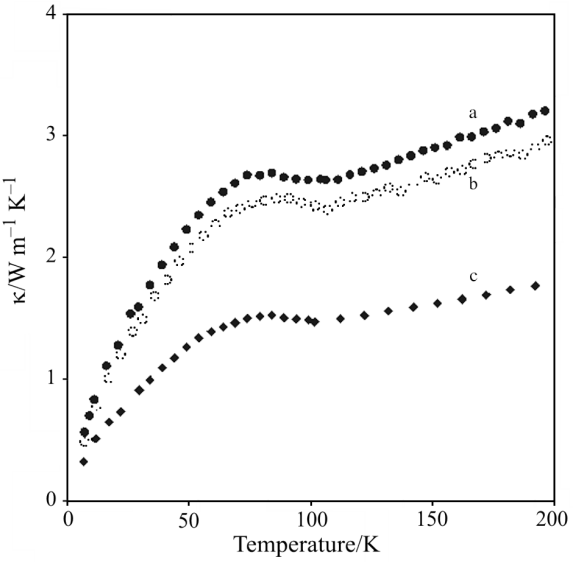

Fig. 5 Corrected $\kappa(T)$ curves of several rods with different volume content of Bi-free non-superconducting precipitates: 6.8% (sample a), 4.9% (sample b) and 0% (sample c)

Thermal conductance of the superconducting module

As mentioned before, the value of the heat load at the cold end of a hybrid HTS/metal current lead is an important technical specification. Therefore, it has to be determined in the current lead prototype under construction. In static (zero current) conditions, the heat load to the helium bath depends exclusively on the low-temperature part of the lead. The temperature of the connection to the metallic part must be kept constant by refrigeration of the resistive (metallic) part to avoid thermal fluctuations and superconductor quench. According to CERN specifications, this temperature should be 50 K. Then, the heat load at the cold end of one superconducting module can be calculated from direct integration of its $K(T)$ function between 4.2 (liquid helium) and 50 K. In operating conditions (600 A of driving current), this heat load increases by the dissipation at the electrical connections to the resistive part of the lead (high-T end), and to the superconducting magnet (low-T end). Eventually, this load is planned to be reduced by refrigeration, most probably from the helium evaporation of the bath.

Superconducting module

A detailed description of the whole lead (metallic and superconducting parts) can be found in [4]. Briefly, the superconducting part of the lead is formed by two

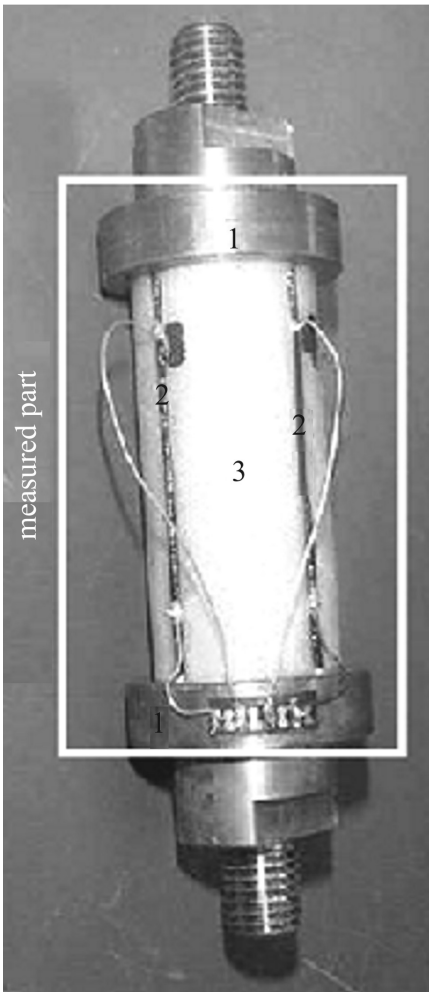

Fig. 6 Photograph of one superconducting module showing the 1 – OFHC copper rings, 2 – the Bi-2212 rods and 3 – the fiberglass, under which the stainless steel shunt is placed. The white rectangle points out the measured part. The electric wires were not placed during the K measurements

pairs of superconducting modules for driving the current in and out of the superconducting magnet. A photograph of one superconducting module is shown in Fig. 6. It consists of four Bi-2212 thin rods of about 1.6 mm in diameter and 10 cm in length, supported by a fibreglass composite tube, which provides stiffness to the assembly. Inside this tube, a stainless steel cylinder of 8 and 12 mm of inner and outer diameter, respectively, has been included as electric shunt, that is, the tube will drive the current in case of superconductor failure. The ends of the shunt and the Bi-2212 rods are soldered to two OFHC copper rings, to provide electrical connection to the high-T and low-T ends. Finally, a copper wire netting has been inserted in the shunt in order to eliminate possible damage occurring during cooling as a consequence of the different thermal expansion coefficients of the Bi-2212 rods (similar to the one of fibreglass) and the stainless steel.

Design features of the big-sized cell

The size of the original commercial thermal conductance cell is not adequate for determining the conductance of current lead modules of more than 22 mm long. For this reason, a new measuring cell (Fig. 1) was designed and manufactured by Termis Ltd. with the largest dimensions permitted by the sealing outer jacket. This new cell allows measuring samples up to 120 mm long and 22 mm in diameter. As in the case of the original cell, the sink and source are two well-polished oxygen-free copper blocks. Radiation shields (not shown) of several dimensions, to cover the whole sample-length range, were also provided to minimize heat losses. These shields are split in two parts to provide a better adjustment and optimize the outer jacket space. Adequate software for measurement control, planning and data acquisition was also supplied.

Relaxation time calculation

The superconducting module contains long Bi-2212 thin rods with low conductivity values. The reaching of stationary measuring conditions is expected to take a long time. In addition, the steady state is not easily detectable because most of the thermal conduction takes part through the stainless steel shunt in parallel with the poor conducting Bi-2212 rods and fibreglass tube, and the long poor conductors have a slow dynamic process. Since the achievement of equilibrium conditions is essential for these measurements, an analytical study of the transitory regime has been carried out to estimate the required measuring time.

The thermal model used for this study is sketched in Fig. 2. The sample, of length L and cross-section A, is placed between the source (x=0) and the sink (x=L). We describe the evolution of the sample temperature $T_s(x,t)$ until reaching a stationary state, which is characterized by a time-independent linear distribution of temperatures. The whole system is initially at a temperature T_{sink}. At t=0, the source is set at T_{source} and a time-dependent heating power $P(t)$ is applied to the source in order to maintain this temperature, compensating for the conduction heat loss through the sample. During the process, the sink is maintained at T=T_{sink}.

This problem starts with the resolution of the one-dimensional equation of heat propagation in a material without heat sources or sinks,

$$a\frac{\delta^2 T_s(x,t)}{\delta x^2} = \frac{\delta T_s(x,t)}{\delta t} \qquad (11)$$

where a is the sample diffusivity, a=$\kappa M_w/C_p d$, M_w is the molecular mass, C_p is the heat capacity, and d, the density. To solve this equation, we use the variable separation method, that is, we assume that it is possi-

ble to separate the contributions of the independent variables into separate functions, each one involving only one independent variable. It gives rise to two differential equations, one first-order and t-dependent, and the other one second-order and x-dependent. The total solution $T_s(x,t)$ is a linear combination of functions, each one being a product of the x- and t-dependent solutions. Then, $T_s(x,t)$ can be expressed as,

$$T_s(x,t)=\sum_{n=0}^{\infty}[X_n(x)Y_n(t)]= \sum_{n=0}^{\infty}\{[A_n\cos(E_n/\sqrt{a})x+B_n\sin(E_n/\sqrt{a})x]\exp(-E_n^2 t)\} \quad (12)$$

where $X_n(x)$ and $Y_n(t)$ are the separate functions involving one independent variable and E_n are the separation constants. This solution assumes that $E_n^2\geq 0$, that is, X_n is periodic in x and Y_n decreases exponentially with time, which agrees which the physics of the problem. Besides, the function $T_s(x,t)$ must verify the initial (13A) and boundary (13B) conditions given by

$$A\rightarrow\begin{cases}T_s(x=0,\,t=0)=T_{source}\\ T_s(x,t=0)=T_{sink},\ x\neq 0\end{cases} \qquad B\rightarrow\begin{cases}T_s(x=0,\,t)=T_{source}\\ T_s(x=L,\,t)=T_{sink}\end{cases} \quad (13)$$

The spatial problem can be directly solved for t=0 by expansion of the function $T_s(x,0)$ (initial condition) in a Fourier series with periodicity 2L. For this purpose and to facilitate the calculation of the Fourier expansion, a new function, $f(x,t)$, is defined as

$$f(x,t)=T_s(x,t)-T_{source}+(\Delta T/L)x \quad (14)$$

where $\Delta T=T_{source}-T_{sink}$. This function is also a solution of Eq. (11) but satisfies different initial and boundary conditions

$$A'\rightarrow\begin{cases}f(x=0,\,t=0)=0\\ f(x,t=0)=\Delta T[(x/L)-1],\ x\neq 0\end{cases} \qquad B'\rightarrow\begin{cases}f(x=0,\,t)=0\\ f(x=L,\,t)=0\end{cases} \quad (15)$$

The new boundary conditions force to extend $f(x,0)$ to be an anti-symmetric function of period 2L

$$\begin{cases}f(x,0)=\Delta T[(x/L)+1],\ -L<x<0\\ f(x,0)=0,\ x=0\\ f(x,0)=\Delta T[(x/L)-1],\ 0<x\leq L\end{cases} \quad (16)$$

which, expanded as a Fourier series, can be written as

$$f(x,0)=-2\sum_{n=1}^{\infty}[(\Delta T/n\pi)\mathrm{sen}(n\pi x/L)] \quad (17)$$

and then, from (14)

$$T_s(x,0)= =T_{source}-(\Delta T/L)x-2\sum_{n=1}^{\infty}[(\Delta T/n\pi)\mathrm{sen}(n\pi x/L)] \quad (18)$$

The values of the separation constants E_n, and the coefficients A_n and B_n can be obtained by comparing Eq. (12) with (18). The function $T_s(x,t)$ can be written as

$$T_s(x,t)=T_{source}-(\Delta T/L)x- -2\sum_{n=1}^{\infty}[\Delta T/n\pi)\mathrm{sen}(n\pi x/L)\exp[-(n\pi/L)^2 at]\} \quad (19)$$

Note that, when $t\rightarrow\infty$, T_s describes a linear distribution along the sample, as expected. Furthermore, from the Newton equation, it is possible to derive an expression for the heating power necessary to maintain T_{source} at x=0

$$P/A=-\kappa_s\left(\frac{\delta T_s(x,t)}{\delta x}\right)_{x=0} \quad (20)$$

where κ_s is the thermal conductivity of the sample. Using Eq. (19),

$$P/A=\kappa_s\left\{(\Delta T/L)+2\sum_{n=1}^{\infty}(\Delta T/L)\exp[-(n\pi/L)^2 at]\right\} \quad (21)$$

and in terms of thermal conductance, $K=\kappa_s A/L$,

$$P(t)=K\Delta T\left\{1+2\sum_{n=1}^{\infty}\exp[-(n\pi/L)^2 at]\right\} \quad (22)$$

From Eq. (22), it is already possible to estimate the relaxation time for a sample, that is proportional to the square of the length and inversely proportional to the thermal diffusivity. Note that the thermal conductance can be derived from this equation taking $t\rightarrow\infty$.

Let us estimate the relaxation time for our Bi-2212 rod at 300 K. Considering the values $\kappa\approx 2.3$ W m^{-1} K^{-1}, $C_p\approx 374$ J mol^{-1} K^{-1} [15], $d\approx 6.6$ g cm^{-3}, and $M_w=888.38$ g mol^{-1}, the thermal diffusivity is $a\approx 8.3\cdot 10^{-3}$ cm^2 s^{-1}. In practice, the stationary state can be considered already reached when the transitory contribution of Eq. (22) is less than 1% of the stationary one. Adding the first 100 terms of the sum, the estimated relaxation time for a sample of 10 cm is about 100 min. Additional terms do not have any significant contribution and Eq. (22) give roughly for the transitory time $t\cong 65L^2$ (t in s, L in cm) in this particular case. The squared length factor indicates a drastic increase of the relaxation time with L.

Measurement results on the current lead module

The thermal conductance of one superconducting module was measured from 5 to 120 K. However, the data obtained must be considered as an upper limit of the

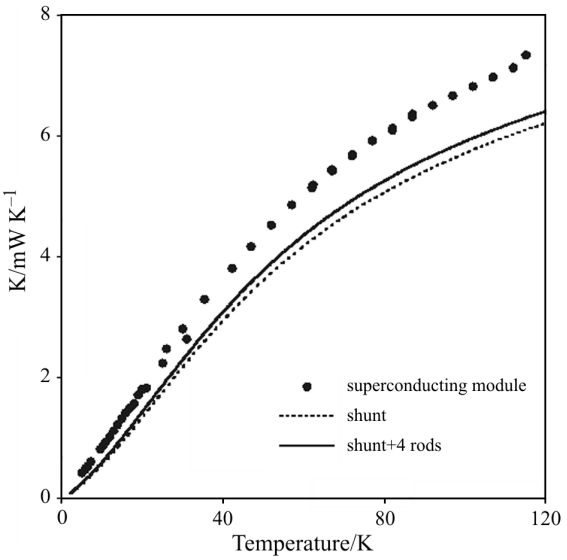

Fig. 7 Measured thermal conductance of one superconducting module, estimated contribution due to the stainless steel shunt and shunt+ the four Bi-2212 rods

real values because no radiation shield was used due to size constraints. Then, some small lateral losses are expected to slightly increase the measured K values.

The dimensions and the thermal conductivity of the shunt and rods taking part of the superconducting module are well known and allow an analytical estimation of the thermal conductance due to the metallic shunt and four Bi-2212 rods. The fibreglass volume and conductivity are not well determined and no estimation is given for this part. The copper connections, junctions and wire netting are not considered either, since their contribution is expected to be small.

The measured K values are depicted in Fig. 7 together with the estimated part described above. The difference between both data series can be mostly assigned to the contributions of the fibreglass. Radiation losses were not minimized but the small values expected and the different shape of the temperature variation given by Eq. (3) precludes any relevant contribution to the excess shown in Fig. 7. The heat load at the cold end, calculated by integrating a fitted curve to the measured data between 4.2 and 50 K

$$P_{\text{load}} = \int_{4.2}^{50} K(T)\mathrm{d}T \tag{23}$$

and considering four modules, is 448 mW. As expected, the major contribution to the overall load comes from the metallic shunt, which should be optimized. In practice, the additional refrigeration provided by the helium gas reduced this heat load to 170 mW in the experimental test [16] realized at CERN in static conditions. In operating conditions the load increased to 210 mW due to power dissipated at the cold-end joints.

The heat load of current lead modules with more complex geometries can be obtained using this set-up, since this magnitude can be calculated from the measured K values is independently of the specimen shape or composition.

Conclusions

We measured the thermal conductivity $\kappa(T)$ of individual Bi-2212 thin rods, as well as the conductance $K(T)$ of the low-T module of a hybrid current lead based on such rods. The commercial set-up used for the thermal conductance measurements follows the steady-state method and covers the range 1.5 to 375 K. Two difficulties were encountered: *i*) The thermal conductivity values of the rods were next to or lower than the set-up lower limit. *ii*) The superconducting module had bigger dimensions than the sample space of the commercial cell.

For the first problem we evaluated the small heat losses taking place during the measurement that represent a negligible contribution for higher K values. The identification of this contribution as radiation losses between source and sink, together with its quantification, allowed calculating an analytical correction function based on the measuring process. The corrected $\kappa(T)$ data for different rods made possible to correlate the obtained κ values with the sample microstructure.

The long and wide size of the superconducting module required to design a new bigger-sized conductance cell with the largest possible dimensions to be inserted in the commercial set-up. In addition, the long Bi-2212 rods of the module, with low diffusivity values, required the analytical calculation of the relaxation time during the measurements, which was estimated to be about 100 min at room temperature for a 10 cm long sample. The measurement of the whole module without radiation shield provided an upper limit for $K(T)$. From this data we estimated a heat load of 448 mW at the cold end of the current lead in static conditions. The comparison of the measured $K(T)$ with the analytical data, calculated taking into account the module dimensions, confirmed the good performance of the newly designed cell and the appropriate estimation of the relaxation time.

Acknowledgements

The authors are indebted to the Spanish Ministerio de Educación y Ciencia and to FEDER for financial support through the projects MAT2004-03395-C02-02 and MAT2002-04121-C03-02. Eva Natividad thanks the Spanish CSIC and the European Social Fund for her I3P contract. L. Garcia-Tabarés and collaborators are also thanked for providing the current lead.

References

1 P. F. Hermann, Current Leads. In: B. Seeber, Ed., Handbook of Applied Superconductivity, IOP Publishing 1998, p. 801.
2 S. Yamaguchi, T. Yamaguchi, K. Nakamura, Y. Hasegawa, H. Okumura and K. Sato, Rev. Sci. Instrum., 75 (2004) 207.
3 A. Ballarino, IEEE Trans. Appl. Supercond., 9 (1999) 523.
4 L. García-Tabarés, J. Calero, P. Abramian, F. Toral, L. A. Angurel, J. C. Díez, R. Burriel, E. Natividad, R. Iturbe and J. Etxeandía, IEEE Trans. Appl. Supercond., 11 (2000) 2543.
5 L. A. Angurel, G. de la Fuente, A. Badía, A. Larrea, J. C. Díez, J. I. Peña, E. Martínez and R. Navarro, Textured BSCCO Superconductors Obtained Via Laser Induced Directional Solidification. In: A. V. Narlikar, Ed., Studies of High Temperature Superconductors Vol. 21, Nova Science Publishers Inc 1997, p. 1.
6 F. Pavese and V. M. Malyshev, Adv. Cryogenic Eng., 40 (1994) 119.
7 D. R. Lide, Ed., Handbook of Chemistry and Physics, CRC Press, 84th Edition, 2003–2004.
8 K. R. Kanter, Derev. Prom., 6 (1957) 17.
9 E. Natividad, M. Castro, R. Burriel, L. A. Angurel, J. C. Díez and R. Navarro, Supercond. Sci. Technol., 15 (2002) 1022.
10 B. Zeini, A. Freimuth, B. Büchner, M. Galffy, R. Gross, A. P. Kampf, M. Kläser, G. Müller-Voght and L. Winkler, Eur. Phys. J., B 20 (2001) 189.
11 K. Khrishana, N. P. Ong, Q. Li, G. D. Gu and N. Koshizuka, Science, 277 (1997) 83.
12 M. Matsukawa, F. Tatezaki, K. Noto, H. Fujishiro, K. Michishita and Y. Kubo, Cryogenics, 34 (1993) 685.
13 P. F. Herrmann, C. Albrecht, J. Bock, C. Cottevieille, S. Elschner, W. Herkert, M.-O. Lafon, H. Lauvray, A. Leriche, W. Nick, E. Preisler, H. Salzburger, J.-M. Tourre and T. Verhaege, IEEE Trans. Appl. Supercond., 3 (1993) 876.
14 S. Nakamae and J. Schwartz, IEEE Trans. Appl. Supercond., 7 (1997) 1699.
15 T. Hasegawa, H. Ikuta and K. Kitasawa, Physical Properties of High Temperature Superconductors III, D. M. Ginsberg Ed., World Scientific, Singapore 1992.
16 A. Ballarino, Physica C: Superconductivity, 372–376 (2002) 1413.

Received: August 12, 2005
Accepted: November 11, 2005

DOI: 10.1007/s10973-005-7293-4